Binari, and K. J. Sleger for helpful discussions, D. Shupe and H. Hier of Allied-Signal Aerospace for the material growth, and J. Mittereder and W. Moore for technical assistance.

24th September 1991

W. Kruppa (*SFA, Inc., Landover, MD 20785, USA*)

J. B. Boos (*Naval Research Laboratory, Washington, DC 20375, USA*)

References

1 PALMATEER, L. F., TASKER, P. J., SCHAFF, W. J., NGUYEN, L. D., LEPORE, A. N., and EASTMAN, L. F.: 'Observation of excess gate current due to hot electrons in 0·2 μm gate length, 100 GHz f_T AlInAs/GaInAs/InP MODFETs'. Inst. Phys. Conf. Ser. No. 96, 1988, pp. 449–454

2 CHEN, Y. K., RADULESCU, D. C., WANG, G. W., NAJJAR, F. E., and EASTMAN, L. F.: 'Observation of high-frequency high-field instability GaAs/InGaAs/AlGaAs DH-MODFETs at K-band', *IEEE Electron Device Lett.*, 1988, **EDL-9**, pp. 1–3

3 LASKAR, J., KETTERSON, A. A., BAILLARGEON, J. N., BROCK, T., ADESIDA, I., CHENG, K. Y., and KOLODZEY, J.: 'Gate-controlled negative resistance in drain current characteristics of AlGaAs/InGaAs/GaAs pseudomorphic MODFETs', *IEEE Electron Device Lett.*, 1989, **EDL-10**, pp. 528–530

4 HO, P., KAO, M. Y., CHAO, P. C., DUH, K. H. G., BALLINGALL, J. M., ALLEN, S. T., TESSMER, A. J., and SMITH, P. M.: 'Extremely high gain 0·15 μm gate-length InAlAs/InGaAs/InP HEMTs', *Electron. Lett.*, 1991, **27**, pp. 325–326

5 DUH, K. H. G., CHAO, P. C., HO, P., TESSMER, A., LIU, S. M. J., KAO, M. Y., SMITH, P. M., and BALLINGALL, J. M.: 'W-band InGaAs HEMT low noise amplifiers'. IEEE MTT-S Int. Microwave Symp. Dig., 1990, pp. 595–598

6 KUANG, J. B., TASKER, P. J., WANG, G. W., CHEN, Y. K., EASTMAN, L. F., AINA, O. A., HIER, H., and FATHIMULLA, A.: 'Kink effect in submicrometer-gate MBE-grown InAlAs/InGaAs/InAlAs heterojunction MESFETs', *IEEE Electron Device Lett.*, 1988, **EDL-9**, pp. 630–632

SiGe WAVEGUIDE PHOTODETECTORS GROWN BY RAPID THERMAL CHEMICAL VAPOUR DEPOSITION

B. Jalali, A. F. J. Levi, F. Ross and E. A. Fitzgerald

Indexing terms: Photodetectors, Vapour deposition, Semiconductor devices and materials

Epitaxial Si/SiGe quantum well waveguide *pin* photodiodes are grown using rapid thermal chemical vapour deposition. Devices with area of $10 \times 1000\,\mu m^2$ have a measured dark current of less than 10 pA at -5 V bias and an external quantum efficiency of approximately 5% at 1 Gbit/s for incident radiation of wavelength $\lambda = 0{\cdot}96\,\mu m$.

The impending use of optical interconnects in future high speed computing and communication systems underscores the need for inexpensive, reliable, optical transmitters and receivers. Because of its maturity and low substrate cost, silicon technology is an obvious choice for such applications. Although the realisation of practical light emitting devices is hindered by the indirect bandgap of silicon, useful optical detection may be achieved. Furthermore, the long wavelength limit of optical absorption in silicon can be extended using SiGe alloys with lower energy gap than pure silicon [1]. In addition, owing to the higher refractive index of Ge, SiGe/Si structures are natural waveguides [2, 3]. This property, may be used in making *pin* waveguide photodetectors in which light propagates normal to the direction of current flow [4–6]. In such structures, a thin (1–5 μm) intrinsic layer results in a short photocurrent transit delay, and the device length may be kept long to compensate for the low absorption coefficient in the indirect bandgap SiGe alloy. We report our preliminary results on the first infra-red waveguide detectors grown by rapid thermal chemical vapour deposition (RTCVD). Diodes with $Si_{0{\cdot}28}Ge_{0{\cdot}72}$/Si multiquantum well intrinsic layers and area of $10 \times 1000\,\mu m^2$ show dark currents of 3 and 8 pA at -1 and -5 V bias, respectively. We also present our initial *pin* detector eye diagrams at 1 Gbit/s for incident light of wavelength $\lambda = 0{\cdot}96$ and $\lambda = 1{\cdot}3\,\mu m$.

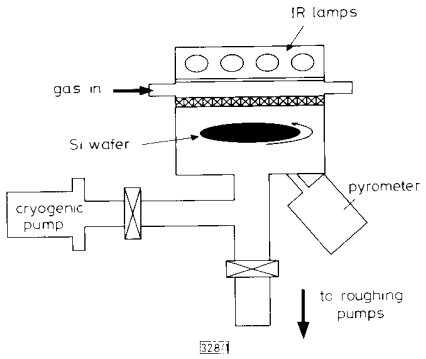

Fig. 1 *Schematic diagram of Rapro RTCVD growth chamber used for crystal growth*

Fig. 1 shows a schematic drawing of the Rapro RTCVD system used for crystal growth. The reactor consists of a water cooled stainless steel outer chamber with quartz internal lining, a quartz shower head for uniform distribution of process gases, tungsten–halogen lamps for rapid heating of the sample, wafer positioning and rotation mechanisms, and an optical pyrometer. A cryogenic pump is used to obtain a low base pressure of 2×10^{-8} torr, and roughing pumps are used to handle large gas volumes during processing. Because growth rate and Ge incorporation must be carefully controlled, and also to avoid three dimensional growth [7], the layers forming an $Si_{1-x}Ge_x$/Si heterostructure are grown at different temperatures. The rapid thermal technique is inherently suitable for growth of such structures with minimum interdiffusion and small processing time per wafer. Table 1 shows the layer structure of the *pin* diode discussed below. The substrates are 4″ in diameter, (100)-oriented, and *n*-type with a resistivity of 0·018 Ω cm. The layer structure consists of a 4000 Å silicon buffer layer, 12 periods of 25 Å strained layer $Si_{0{\cdot}28}Ge_{0{\cdot}72}$ quantum wells sandwiched between 550 Å silicon followed by 2000 Å *p*-type silicon with an impurity concentration $p = 1 \times 10^{19}\,cm^{-2}$. The SiGe layers were grown at 500°C using GeH_4 and $Si_2Cl_2H_2$ gases and the silicon barriers were grown at 800°C using $Si_2Cl_2H_2$ both at a pressure of 4 torr. The growth temperature for the SiGe layers was chosen to ensure smooth two dimensional growth [7], and their thickness was kept within the equilibrium critical thickness [8]. The latter ensures that the strained layers remain stable during subsequent processing. Fig. 2*a* shows a cross-sectional transmission electron microscope (TEM) photograph of the device after fabrication. Fig. 2*b* is a similar structure with 140 Å $Si_{0{\cdot}65}Ge_{0{\cdot}35}$ quantum wells. TEM analysis showed no misfit dislocations on either structures. After growth, waveguide diodes were fabricated using conventional processing techniques. The 10 μm wide mesa structures were formed by reactive ion etching and passivated using deposited SiO_2.

Table 1 LAYER STRUCTURE OF *pin* PHOTODIODE

	Layer	Thickness
		Å
	P^+ Si	1500
	i-Si	2000
12 periods	$i - Si_{0{\cdot}28}Ge_{0{\cdot}72}$	25
	i-Si	550
	i-$Si_{0{\cdot}28}Ge_{0{\cdot}72}$	25
	i-Si	4000
	n^+-Si Substrate	

Fig. 3*a* shows the breakdown characteristics of a typical device. The breakdown voltage is 42 V and is consistent with the expected value for a similar structure of pure silicon. The uniformity of the breakdown voltage across the wafer is excellent with a measured variation of only ± 1 V. Fig. 3*b* exhibits the current–voltage characteristics for a device of area $10 \times 1000\,\mu m^2$. The device exhibits dark currents of 3 pA at -1 V, 8 pA at -5 V, and 30 pA at -30 V. The fact that the leakage currents are so small demonstrates the high quality of the material from which the devices are fabricated. In comparison to early results [4, 5], our dark current is lower by five orders of magnitude. Such low dark currents are very important for realisation of low noise lightwave receivers. The inset in the Figure shows a scanning electron micrograph for part of an 18 wide array of these detectors. Because light is coupled horizontally to these devices, they are inherently suitable for one dimensional receiver arrays in optical data link (ODL) applications.

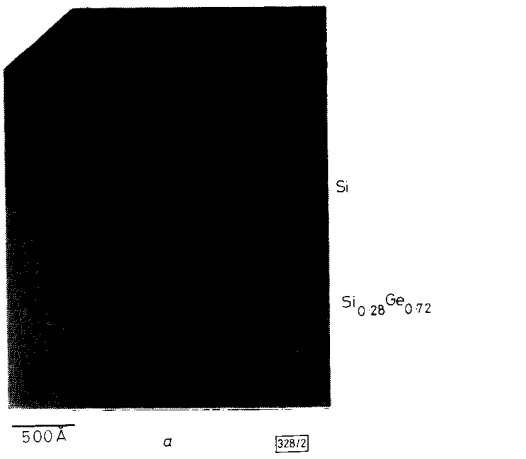

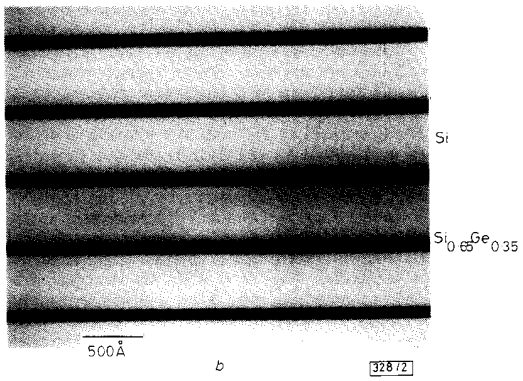

Fig. 2 *TEM cross-section of 25 Å $Si_{0.28}Ge_{0.72}$ quantum wells, and 140 Å $Si_{0.65}Ge_{0.35}$ quantum well sandwiched between 550 Å Si barrier layers grown by RTCVD*

a $Si_{0.28}Ge_{0.72}$
b $Si_{0.65}Ge_{0.35}$

The optical response of the devices discussed above is measured by coupling light from a laser diode via a lensed multimode fibre into the cleaved edge of the *pin*. In Fig. 4 we show the eye diagram for a 1 Gbit/s digital nonreturn-to-zero pseudorandom optical data stream incident on the *pin*. Average input optical power is 1 mW and the wavelength of optical radiation used is $\lambda = 0{\cdot}96\,\mu m$. In Fig. 5 we show the amplified ($\times 100$) response of the *pin*. In this situation external efficiency of the *pin* is about 5%. This value may be improved by increasing optical confinement in the structure by, for example increasing the thickness of the *i*-Si layer (see Table 1). The ultimate response time of the detector is limited by the 4 pF capacitance of the device which includes a large contribution from a metal bondpad used to make electrical contact to the p^+ layer.

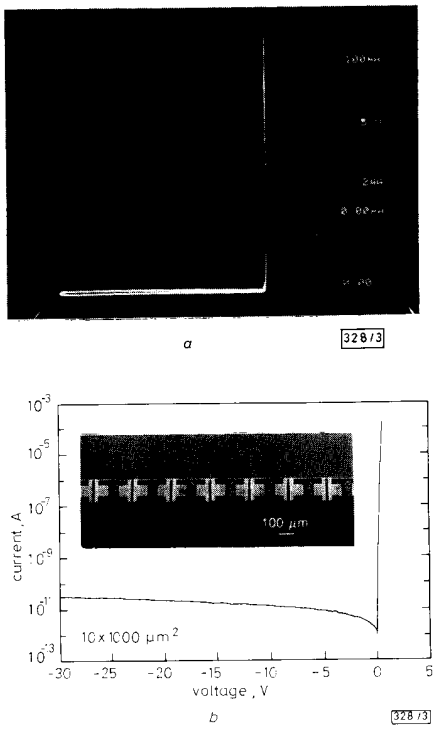

Fig. 3 *Measured breakdown characteristics of Si/SiGe pin diode and current–voltage characteristics of $Si/Si_{0.28}Ge_{0.72}$ pin diode*

a Breakdown characteristics of Si/SiGe *pin*
Breakdown voltage is 42 V
b Current–voltage characteristics of $Si/Si_{0.28}Ge_{0.72}$ *pin*
Inset: SEM image of 18 wide Si/SiGe *pin* array with 250 μm lateral spacing between detectors

In Fig. 6 we show the amplified ($\times 1000$) response of a Si/SiGe *pin* to a $\lambda = 1{\cdot}3\,\mu m$ 1 Gbit/s random data stream. Although this structure has not been optimised for detecting radiation at $\lambda = 1{\cdot}3\,\mu m$ the external efficiency of the *pin* is better than 0·1%.

In summary, we have demonstrated the utility of rapid thermal chemical vapour deposition for epitaxial growth of Si/SiGe quantum well *pin* photodiode structures. Our devices have measured dark currents of less than 10 pA at -5 V bias

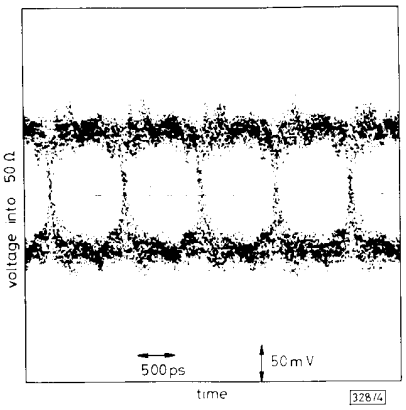

Fig. 4 *1 Gbit/s $\lambda = 0{\cdot}96\,\mu m$ input eye diagram*

and show useful response to 1 Gbit/s, $\lambda = 0{\cdot}96\,\mu m$ optical signals. With further improvements we expect such structures to be used in monolithic silicon optoelectronic receivers.

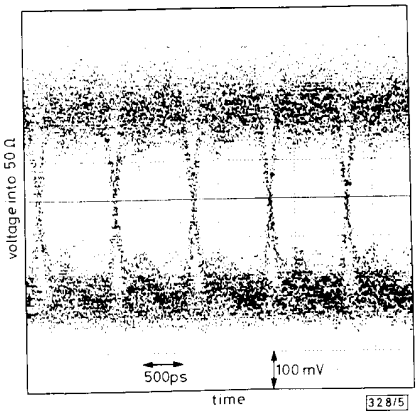

Fig. 5 *Detected 1 Gbit/s eye diagram*
Voltage scale is × 100 into 50 Ω
Si/SiGe *pin* is reverse biased at −1 V

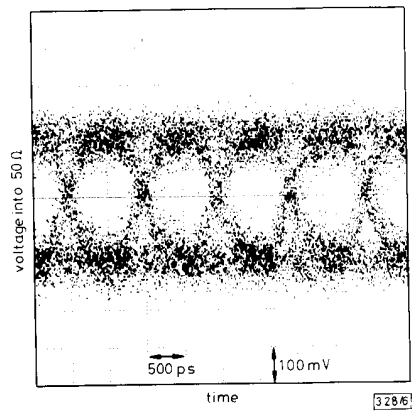

Fig. 6 *× 1000 response of Si/SiGe pin at $\lambda = 1{\cdot}3\,\mu m$*
pin is reverse biased at −12 V

Acknowledgments: We would like to thank T. Sorsch and M. Anzlowar for technical assistance, B. Weir for RBS analysis, and R. A. Soref for helpful discussions.

18th November 1991

B. Jalali, A. F. J. Levi, F. Ross and E. A. Fitzgerald (*AT&T Bell Laboratories, 600 Mountain Ave., Murray Hill, NJ 07974, USA*)

References

1 LURYI, S., KASTALSKY, A., and BEAN, J. C.: 'New infrared detector on a silicon chip', *IEEE Trans.*, 1984, **ED-9**, (9), pp. 1135–1139
2 LURYI, S., PEARSALL, T. P., TEMKIN, H., and BEAN, J. C.: 'Waveguide infrared photodetectors on a silicon chip', *IEEE Electron Device Lett.*, 1986, **EDL-7**, (2), pp. 104–106
3 SOREF, R. A., NAVAMAR, F., and LORENZO, J. P.: 'Optical waveguiding in a single-crystal layer of germanium silicon grown on silicon', *Opt. Lett.*, 1990, **15**, (5), pp. 270–272
4 PEARSALL, T. P., TEMKIN, H., BEAN, J. C., and LURYI, S.: 'Avalanche gain in Ge_xSi_{1-x}/Si infrared waveguide detectors', *IEEE Electron Device Lett.*, 1986, **EDL-7**, (5), pp. 330–332
5 TEMKIN, H., PEARSALL, T. P., BEAN, J. C., LOGAN, R. A., and LURYI, S.: 'Ge_xSi_{1-x} strained-layer superlattice waveguide photodetectors operating near 1·3 μm', *Appl. Phys. Lett.*, 1986, **48**, (55), pp. 963–965
6 KESAN, V. P., TREYZ, G. V., MAY, P. G., IYER, S. S., and HALBOUT, J. M.: 'Integrated rib-waveguide Si/SiGe photodetector for long wavelengths'. Proc. CLEO, Baltimore, Md., 13th–17th May 1991
7 BEAN, J. C., SHENG, T. T., FELDMAN, L. C., FIORY, A. T., and LYNCH, R. T.: 'Pseudomorphic growth of Ge_xSi_{1-x} on silicon by molecular beam epitaxy', *Appl. Phys. Lett.*, 1984, **44**, (1), pp. 102–104
8 MATHEWS, J. W., and BLAKESLEE, A. E.: *J. Cryst. Growth*, 1974, **27**, pp. 118–125

REMOTE FIBRE-OPTIC AC MAGNETOMETER

A. R. Davis, S. S. Patrick, A. Dandridge and F. Bucholtz

Indexing terms: Fibre-optics, Optical sensors

A remotely operated fibre-optic magnetometer was fabricated and tested. The system has a real time flat frequency response (±3 dB) across the entire band of 1–45 kHz with a minimum detectable magnetic field of $1{\cdot}8 \times 10^{-7}$ Gauss/$\sqrt{(Hz)}$. The sensor is compact and contains no electronic or active components.

Introduction: Fibre-optic AC magnetic field sensors have been reported that use the Faraday effect [1], the magnetostrictive effect [2] and the Lorentz force effect [3]. In general, these sensors have exhibited either large bandwidth and low resolution or medium-to-high resolution with strong in-band variations in the frequency response. In some cases active elements were required in the transducer either for magnetic biasing or for interferometer stabilisation. We describe a magnetostrictive sensor for the measurement of AC magnetic fields. The transducer is totally passive in nature, shows flat (±3 dB) response over the frequency range 1–45 kHz, and exhibits resolution of $1{\cdot}8 \times 10^{-7}$ G/$\sqrt{(Hz)}$ over the entire frequency range.

The magnetostriction of metallic glasses e for small fields is given by $e = C_{eff}H^2$ [4] where H is the total applied magnetic field and C_{eff} is a material parameter. If a DC magnetic field H_0, is applied to a magnetostrictive sensor via a permanent magnet, the applied field becomes $H = H_0 + H_\omega$ is the AC field of interest at some frequency ω. Substituting this for H, the magnetostriction becomes

$$e = C_{eff}(H_0^2 + 2H_0H_\omega + H_\omega^2) \quad (1)$$

A fibre-optic interferometric sensor constructed of magnetostrictive material would have a phase shift at the frequency ω of $\phi_\omega = 2l\alpha CH_0H_\omega$ where l is the length of fibre wound on the sensor, $\alpha = 2\pi n(0{\cdot}78)/\lambda$, n is the optical index of the fibre and λ is the optical wavelength. This phase shift is the signal of interest.

Eqn. 1 shows that there will be additional phase shifts generated at DC and 2ω. The phase shift induced at DC is irrelevant in an AC interferometric sensor system; however, the signal at 2ω will cause harmonic distortion with a level of

$$HD = 20\log[H_\omega^2/2H_0H_\omega] = 20\log[H_\omega/2H_0] \quad (2)$$

Thus, for a harmonic distortion of −60 dB, the largest AC field which can be measured must be below 0·2% that of the DC 'bias' field. For a bias field of 10 Gauss, this corresponds to a signal of 20 mGauss.

To achieve remote operation, one of several interferometric phase retrieval techniques must be employed. These include, but are not limited to, phase generated carrier [5], and active homodyne feedback to source wavelength [6].

Experiment: The sensors were fabricated from unannealed Allied Metglas 2605 S2 ($Fe_{78}B_{13}Si_9$) strips 25 mm wide and 25 μm thick. These were formed into cylinders 12 mm in diameter. The cylinders were tension wound with 7 m of 80 μm diameter payout fibre which covered 90% of the cylinder length with a single layer. A permanent magnet 3 mm square